




An insight into the suitability of magnesium ion-conducting biodegradable methyl cellulose solid polymer electrolyte film in energy storage devices

Jayalakshmi Koliyoor^{1,2}, Ismayil^{2,*} , Shreedatta Hegde³, Ganesh Sanjeev³, and Mudiya Subrahmanya Murari⁴

¹Department of Sciences, Manipal Academy of Higher Education, Manipal, Karnataka 576104, India

²Department of Physics, Manipal Institute of Technology, Manipal Academy of Higher Education, Manipal, Karnataka 576104, India

³Department of Physics, Mangalore University, Mangalagangothri, Karnataka 574199, India

⁴DST-PURSE Program, Mangalore University, Mangalagangothri, Karnataka 574199, India

Received: 14 November 2022

Accepted: 27 February 2023

Published online:

14 March 2023

© The Author(s) 2023

ABSTRACT

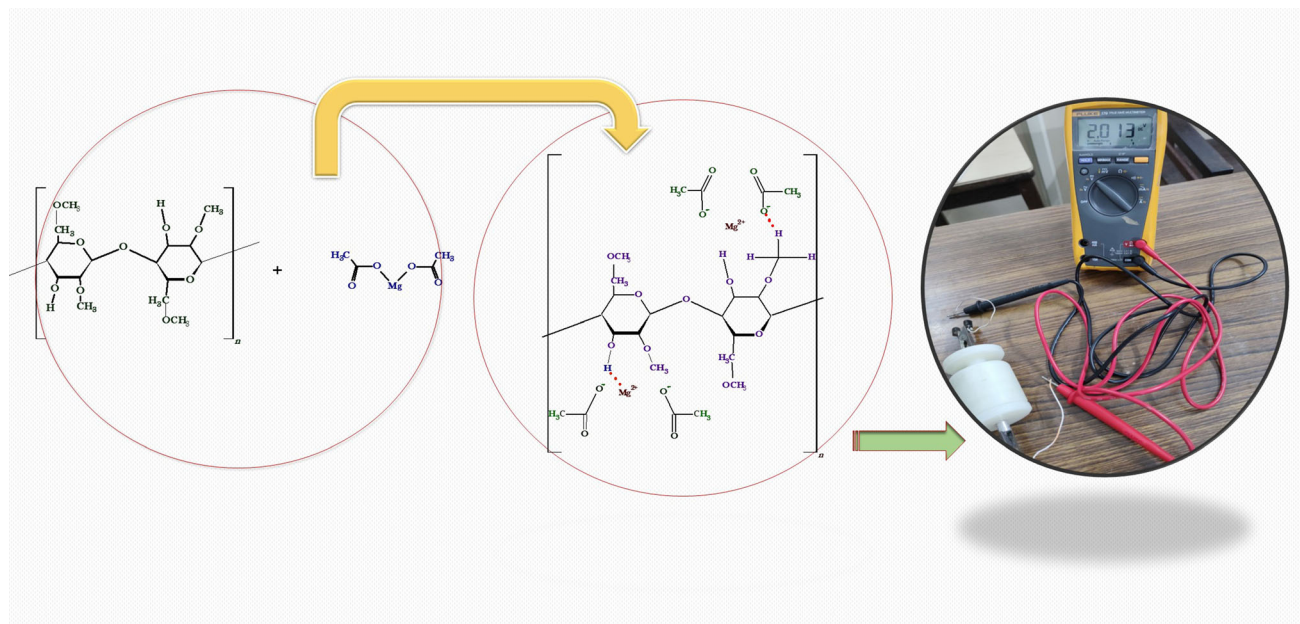
Biodegradable solid polymer electrolyte films based on methyl cellulose and magnesium acetate tetrahydrate $[\text{Mg}(\text{CH}_3\text{COO})_2 \cdot 4\text{H}_2\text{O}]$ are prepared using the conventional solution casting technique. Structural analysis of the electrolyte films confirmed the complexation of salt with the polymer matrix. The incorporation of salt into the polymer matrix resulted in the enhancement of the amorphousness of the matrix. The thermal properties of the electrolyte film are analyzed with the help of DSC and TGA thermograms. Impedance analysis of the films indicates the enhancement of the electrical conductivity of the system. The maximum room temperature ionic conductivity ($2.61 \times 10^{-5} \text{ S/cm}$) was observed for the 25wt% salt-doped sample. The highest conducting electrolyte system has an Electrochemical Stability Window (ESW) of 3.47 V. In the current work, a primary battery was assembled using the highest conducting polymer electrolyte system, and its open-circuit potential and discharge characteristics were also investigated.

Handling Editor: Maude Jimenez.

Address correspondence to E-mail: ismayil.mit@manipal.edu; ismayil.486@gmail.com

<https://doi.org/10.1007/s10853-023-08355-0>

GRAPHICAL ABSTRACT



Introduction

Energy storage devices have become an integral part of life in the past few years. They have played a crucial role in the advancement of technology. Electrolytes, the decisive component of energy storage devices, have recently been a hot topic for research [1–3]. The electrolyte is very vital in defining the properties of these energy storage devices [4]. Among the different classes of electrolytes, polymer electrolytes have certain advantages compared to other electrolytes, such as good mechanical stability and high electrolyte–electrode interfacial stability. [5]. Polymer electrolytes can be efficiently used in modern applications [5]. These are further classified into solid polymer electrolytes (SPE), gel polymer electrolytes (GPE), blend polymer electrolytes (BPE), and composite polymer electrolytes (CPE) [6]. However, ease of preparation and excellent mechanical, chemical, and thermal stabilities have tremendously affected the study of SPEs. Several works can be found on different SPEs in the literature [7–14].

Despite having several advantages, polymer electrolytes have a few disadvantages that might hinder

the usage of these electrolytes in energy storage devices. There are two significant points of concern. The main challenge is the low ionic conductivity, especially in comparison with Lithium-ion batteries that are commercially used [15]. This shortcoming can be overcome by incorporating the nanofiller into the polymer electrolyte matrix. The second matter of concern is the high electrode–electrolyte resistance which results in poor interfaces. This can be overcome by employing adhesives in the electrolyte matrix [15].

Generally, SPEs are prepared by incorporating a metal salt into the polymer matrix [4, 16]. To date, different ion-conducting polymer electrolytes have been studied extensively: lithium-ion, sodium-ion, and magnesium-ion conducting polymer electrolytes [4]. Even though an extensive study has been carried out on Li-ion conducting electrolytes, Li-ion has certain disadvantages, such as low abundance, high reactivity, and dendrite growth. [17]. Magnesium can overcome these limitations due to its low reactivity, high abundance, and enhanced volumetric capacity compared to lithium [18].

Although initial research was mainly concentrated on lithium-ion batteries, the recent trend has shifted to multivalent ions, especially magnesium, due to their superior characteristics. Magnesium ion can be

employed in energy storage devices in liquid or solid electrolyte forms. But the development of passive layer formation at the electrode–electrolyte interface poses a severe challenge to the commercial application of liquid electrolytes, thereby hindering their stability [19]. Recent years have witnessed tremendous work on polymer-based magnesium ion batteries. Manjuladevi et al. prepared a primary battery employing the solid polymer electrolyte films based on PVA/PAN-magnesium chloride [20] and observed an open-circuit potential of 2.17 V. Polu et al. developed a primary battery based on PVA and magnesium acetate and observed an OCV of 1.84 V [21]. Priya et al. have analyzed the suitability of I-carrageenan-based magnesium ion electrolytes in primary battery applications and observed an OCV of 2.17 V. similar studies also can be found in the literature [22–25].

Along with the dopant, the nature of the polymer matrix is also essential in deciding the characteristics of the electrolyte systems. Various electrolyte systems have been developed using biodegradable polymers as a dissolving matrix and were found to have good electrical, structural, and thermal properties [8, 26, 27]. Hamsan et al. [28] prepared protonic conducting plasticized methyl cellulose-potato starch based electrolyte films and analyzed the rechargeability of the protonic cell. Aziz et al. prepared a biodegradable solid polymer electrolyte based on chitosan and methyl cellulose polymer blend and investigated their suitability for electric double-layer capacitor (EDLC) applications [29]. Hamsan et al. prepared proton-conducting green polymer electrolyte films based on Dextran extracted from *Leuconostoc mesenteroides*. They observed a maximum room temperature conductivity of $(1.15 \pm 0.08) \times 10^{-3}$ S/cm [30]. Considering the present global situation, it is necessary to shift toward biodegradable polymers as a dissolving matrix for electrolyte systems [31]. Taking this into account, in the present work, we have prepared a biodegradable solid polymer electrolyte based on methyl cellulose incorporated with magnesium acetate salt.

Methyl cellulose is a cellulose derivative with 27.5–31.5% of methoxy groups [32]. It has good thermal and mechanical stability, and also it has good film-forming ability [33]. Due to its versatile property, methyl cellulose can be used in various applications [34, 35]. Methyl cellulose can also be an efficient candidate for preparing polymer electrolytes, as

evident from the literature [36–40]. Given its popularity, this study chose methyl cellulose as a polymer matrix. The proposed work accounts for the structural, electrical, and thermal properties of the biodegradable solid polymer electrolytes based on methyl cellulose and magnesium acetate tetrahydrate $[\text{Mg}(\text{CH}_3\text{COO})_2 \cdot 4\text{H}_2\text{O}]$. In addition, the open circuit and discharge characteristics of a primary battery constructed with the highest conducting electrolyte have been presented.

Materials and methodology

Materials used

Methyl Cellulose (viscosity: 350–550 cps) and magnesium acetate tetrahydrate, $\text{Mg}(\text{CH}_3\text{COO})_2 \cdot 4\text{H}_2\text{O}$ (molecular weight: 214.45 g/mol) were procured from Loba Chemie Pvt. Ltd., Mumbai, and were used as such.

Sample Preparation

Solid polymer electrolyte films were prepared using the solution casting method. Different amounts of methyl cellulose and magnesium acetate tetrahydrate salt totaling 2g were weighed according to Eq. (1) and dissolved in water [41].

$$M(\text{wt}\%) = \frac{m_d}{m_p + m_d} \times 100\% \quad (1)$$

where m_d and m_p represent the dopant salt's weight and polymer's weight, respectively.

The solution was stirred into a homogeneous mixture for 10 h at 45 °C. This mixture was poured into Petri dishes and evaporated slowly at a constant temperature. Obtained solvent-free films were peeled off and kept in a hot air oven for 24 h to remove the traces of water. The thickness of the films varied between 50 and 100 μm . The films were designated as shown in Table 1. Free-standing films were not obtained above 30% weight percentage of salt irrespective of several attempts due to the excess salt.

Characterization techniques

FTIR analysis of the electrolyte films was carried out with the help of the Shimadzu IR SPIRIT ATR-FTIR spectrometer. The spectra were recorded between 400 and 4000 cm^{-1} with a resolution of 4 cm^{-1} . Structural

Table 1 Designation of the electrolyte films

Methyl Cellulose (wt%)	Magnesium acetate tetrahydrate (wt%)	Designation
100	0	MAC0
95	5	MAC5
90	10	MAC10
85	15	MAC15
80	20	MAC20
75	25	MAC25
70	30	MAC30

properties were studied with the help of the Rigaku miniflex 5th generation XRD spectrometer. The films were subjected to Cu-K α X-ray radiation in the range of 5°–80° with a step size of 2°/min. SEM micrographs were obtained from CARLZEESIS Scanning Electron Microscope (SEM). DSC studies were carried out with the help of Shimadzu DSC 60 plus. The films were placed in the nitrogen atmosphere in the aluminum pan and heated at 10 °C/min. TGA thermograms were obtained using Hitachi STA7200 TGA-DTA. Samples were kept in the nitrogen atmosphere and heated from room temperature to 500 °C. Impedance measurements were taken with the help of the Agilent 4294A precision impedance analyzer in the frequency range between 40 Hz–5 MHz. *I*–*V*

characteristics were noted using Keithley source meter 2636B.

Results and discussions

FTIR analysis

The interaction between methyl cellulose and magnesium salt can be analyzed with the help of FTIR studies. FTIR spectra of prepared electrolyte samples are shown in Fig. 1. Table 2 lists the characteristic peaks of the polymer's various functional groups and how they shift with salt incorporation. Magnesium acetate tetrahydrate has six major peaks: A peak around 3524 cm⁻¹ corresponds to O–H stretching [42]. Peaks accounting for asymmetric and symmetric

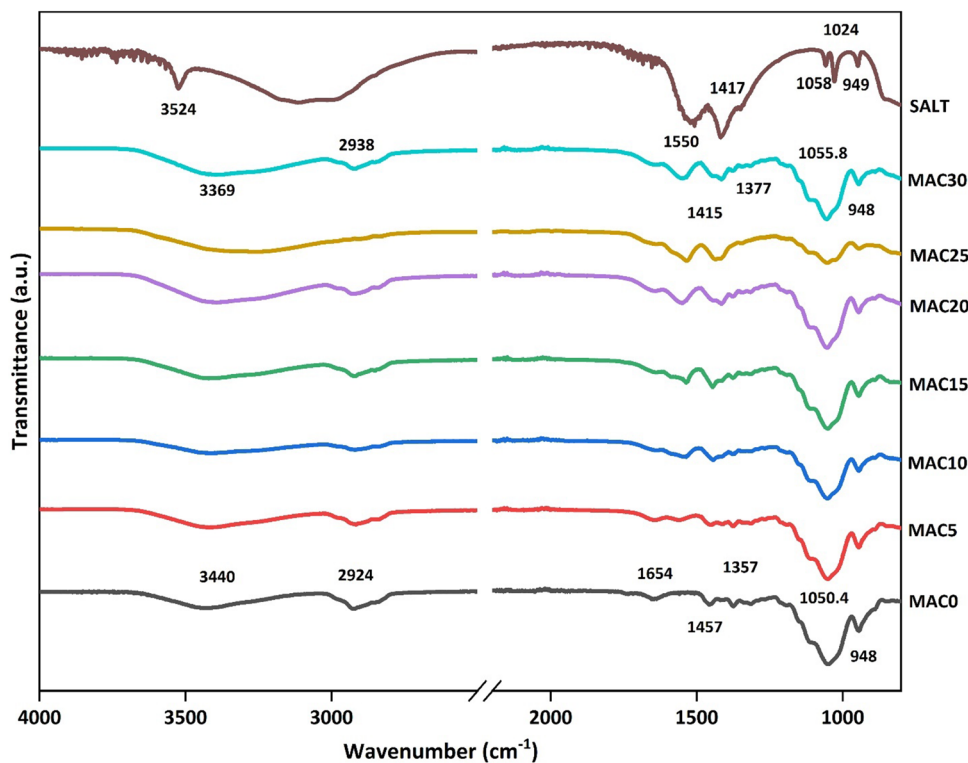
Figure 1 FTIR spectra of pristine and magnesium acetate-doped polymer electrolyte systems.

Table 2 Peak assignments for the peaks observed at different wavenumbers

MAC0	MAC5	MAC10	MAC15	MAC20	MAC25	MAC30	Peak Assignment
3440	3416	3421	3420	3382	3250	3369	O–H stretching[45]
2924	2915	2917	2916	2907	2902	2938	C–H asymmetric stretching [46]
1654	1644	1640.4	1641	1640	1640	1643	O–H bending [46]
1457	1452	1442	1442	1440	1435	1415	Vibration of deformation in $\delta(\text{C–H})$ [46]
1375	1372	1373	1373	1376	–	1377	C–H bending [47]
1050.4	1051.2	1051.3	1052	1053.1	1052.6	1055.8	C–O–C stretching[48]
948	948	948	948	948	948	948	Glycosidic linkage[47]

stretching modes of C–O exist around 1550 cm^{-1} , and 1417 cm^{-1} [43, 43], a peak around 1058 cm^{-1} corresponds to the out-of-plane CH_3 rocking, and the peak corresponding to the in-plane CH_3 rocking is observed around 1024 cm^{-1} [43]. Similarly, a sharp peak around 949 cm^{-1} is due to the C–C stretching [43].

From Table 2, the shift in the peaks corresponding to O–H stretching, C–H asymmetric stretching, and vibration of deformation in $\delta(\text{C–H})$ indicate the interaction between these functional groups of the polymer and the magnesium acetate salt. This is further confirmed by analyzing the variation in the force constant corresponding to these vibrations. The force constant of a given bond can be calculated by using the following expression [8]:

$$\bar{\nu} = \frac{1}{2\pi c} \sqrt{\frac{K}{\mu}} \quad (2)$$

where $\bar{\nu}$ is the wavenumber, K is the force constant, μ is the reduced mass corresponding to the constituents of the bond, and c is the speed of light

Values of force constant corresponding to O–H stretching, C–H asymmetric stretching, and deformation vibration in $\delta(\text{C–H})$ are given in Table 3. It is

evident from Table 3 that with the rise in the salt concentration, the force constant corresponding to these bonds drops down. As the force constant decreases, bond length increases, implying that the bond gets weaker. Generally, the force constant can be related to the bond length. It can be observed from the relation given by Badger [49] that the force constant is inversely proportional to the bond length. Table 3 indicates a decline in the force constant of O–H and C–H bonds with the increase in the salt content. As force constant and bond length are inversely related, bond length increases with the decrease in the force constant. It is evident that as the bond length increases, the strength of the bond decreases, facilitating the complexation of ions of the salt into the polymer matrix. Hence, there is a possibility that the ions of the incorporated salt have interacted with the O–H and C–H bonds of the polymer backbone. The magnesium salt's carboxyl anion (COO^-) interacts with the C–H bond, and Mg^{+2} interacts with the more electronegative O–H bond [8]. This is evident by the decrease in the force constants corresponding to the O–H and C–H bonds of methyl cellulose. A schematic diagram of possible interaction between the polymer matrix and magnesium salt has been drawn and shown in Fig. 2.

Table 3 Variation of force constants of different vibration modes with the salt content

Electrolyte	Force Constant (N/cm)		
	O–H stretching	C–H asymmetric stretching	Vibration of deformation in $\delta(\text{C–H})$
MAC0	6.53	4.65	1.15
MAC5	6.48	4.62	1.15
MC10	6.49	4.63	1.13
MAC15	6.49	4.62	1.13
MAC20	6.35	4.59	1.12
MAC25	5.86	–	1.12
MAC30	6.30	4.69	1.08

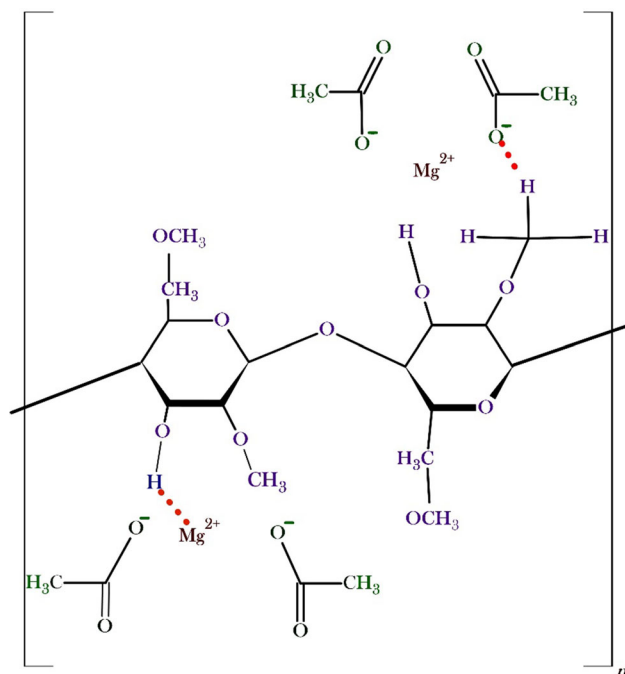


Figure 2 Schematic diagram of probable interaction between methyl cellulose and magnesium acetate salt.

XRD analysis

The variation of crystallinity of the polymer with the incorporation of magnesium salt was studied using XRD analysis. XRD spectra of the prepared polymer electrolytes are given in Fig. 3. MAC0, a pristine polymer, has a sharp peak around $2\theta = 9^\circ$ due to the cellulose matrix modification [47]. An amorphous hump is observed around $2\theta = 10^\circ\text{--}21^\circ$ [50]. As observed from the figure, the intensity of the peak around 20° decreases with the inclusion of the salt, indicating a decrease in the crystallinity of the polymer matrix with the increase in salt. To confirm this, XRD diffractograms were deconvoluted with the help of Fityk software [51] employing the Gaussian function. Deconvoluted graphs of the electrolytes are depicted in Fig. 4. The degree of crystallinity of all the samples was calculated using the following expression [52] and is given in Table 4.

$$X_c = \frac{A_c}{A_c + A_A} \quad (3)$$

where A_c and A_A represent the area under crystalline and amorphous peaks, and from the table, MAC0 has a degree of crystallinity of 24.5%. With the incorporation of the magnesium acetate salt, a slight increase

Figure 3 XRD diffractograms of polymer electrolytes.

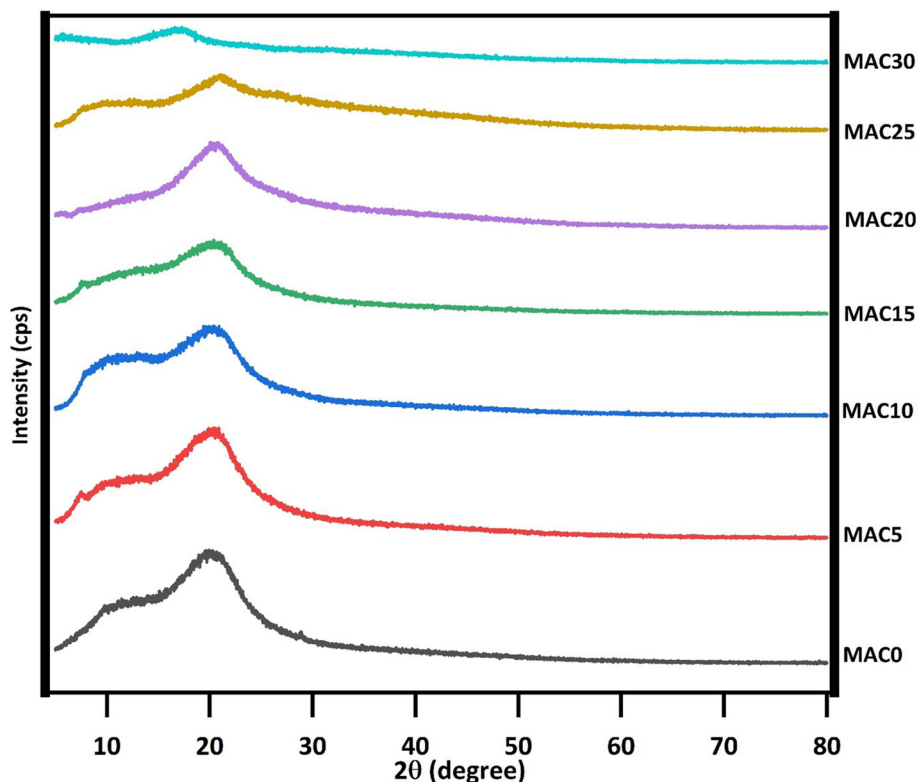
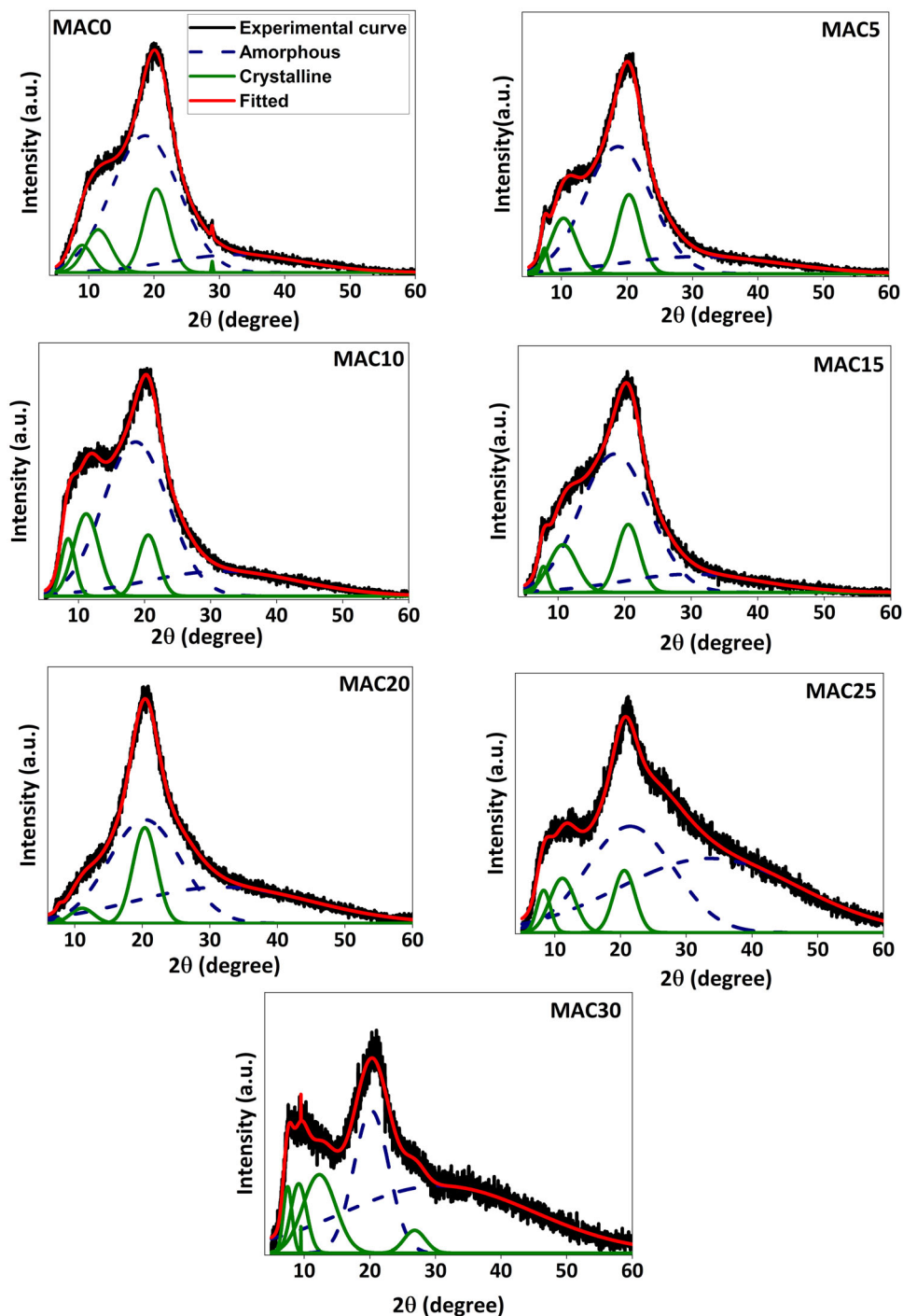


Figure 4 XRD deconvoluted graphs of polymer electrolyte films.



in the crystallinity of the polymer matrix can be observed (from MAC0 to MAC5). This increase in the crystallinity of MAC5 in comparison with MAC0 can be attributed to the self-cross-linkage formation at the lower concentration of magnesium salt. Similar behavior has been reported by Liew et al. [53] and Mazuki et al. [54].

Further, this increase in the crystallinity for MAC5 can be correlated to the decline in its ionic conductivity. Besides, as the salt concentration increases, the crystallinity of the electrolyte films decreases, which is consistent with the impedance analysis. The decline in crystallinity or upsurge in amorphousness of the film with increasing salt concentration is caused by the rupturing of hydrogen bonds in the

Table 4 A_A , A_C , and degree of crystallinity of pristine and salt incorporate polymer electrolytes

Electrolyte	Amorphous area (A_A)	Crystalline area (A_C)	Degree of crystallinity (X_C in %)
MAC0	19,138.0	6207.3	24.5
MAC5	18,206.8	5997.3	24.8
MAC10	18,675.1	5590.0	23.0
MAC15	13,019.5	3346.3	20.4
MAC20	16,235.1	3100.1	16.0
MAC25	18,365.7	2655.0	12.6
MAC30	7534.4	2042.3	21.3

polymer matrix due to electrostatic interaction between the salt ions and the polymer segments [52]. The decrease in the crystallinity enhances the movement of polymer segments, thus accounting for the increase in the ionic conductivity of the electrolyte systems. MAC25, the highest conducting electrolyte system, has the least degree of crystallinity of 12.6%. With further inclusion of salt, for MAC30, a rapid increase in the crystallinity is observed, which might be due to the recrystallization of the polymer matrix [39]. This is also evident from the SEM micrographs.

SEM analysis

SEM micrographs of pristine and salt-doped electrolyte films are given in Fig. 5. The surface of methyl cellulose (MAC0) is smooth and homogeneous [55]. The addition of salt makes the surface rough, and granules of different sizes and shapes can be observed [56]. As a result, an initial decrement in the ionic conductivity can be seen, which can be correlated to a slight increase in the crystallinity of MAC5. With an increase in the salt content, more granules get accommodated on the surface. This is observed up to MAC20. For MAC25, the appearance of large-sized granules in comparison with low salt systems can be observed. The presence of these granules owes to the rapid increase in number density and mobility of the ions, which is in good agreement with calculated transport parameters [39]. SEM micrograph of MAC30 indicates recrystallization of the polymer matrix, which results in the enhancement of crystallinity of the polymer matrix as observed from the XRD studies.

DSC analysis

DSC thermograms of pristine and salt-doped polymer electrolyte systems are given in Fig. 6. The glass transition temperature of the electrolyte films was

found from the thermogram; the values are tabulated in Table 5. MAC0 has a glass transition temperature (T_g) of 43.6 °C. A slight decrease in the T_g of MAC5 can be attributed to an increase in the crystallinity of the matrix [57]. Apart from the initial decrease in T_g , a gradual increase in glass transition temperature is observed with the further inclusion of the salt. This increase in the T_g may be due to the increase in cation coordination with the polymer matrix [44] or due to the expansion of the polymer segments, which is evident from the increase in the amorphousness of the polymer matrix from XRD studies [57]. MAC25, the highest conducting polymer electrolyte from impedance analysis, exhibits a T_g of 60.7 °C. With further inclusion of the salt, the glass transition temperature may decrease due to the formation of ion aggregates, as evidenced by SEM and XRD studies.

TGA analysis

Thermogravimetric (TGA) analysis accounts for understanding the materials' thermal stability. The TGA thermogram of MAC0 and highest conducting MAC25 is shown in Fig. 7. A slight loss in moisture can be observed for MAC0 and MAC25 up to 100 °C, which might be due to the loss of moisture that might be accumulated due to the handling of the samples [58, 59]. Except for the initial weight loss, MAC0 is thermally stable up to 300 °C. Degradation of MAC0 starts around 300 °C, which continues up to 385 °C resulting in a rapid weight loss of up to 80%. This could be because the polymer matrix contains the COO^- group [60].

On the other hand, a small amount of weight loss can be observed in the case of MAC25 up to 130 °C due to the degradation of $\text{Mg}(\text{CH}_3\text{COO})_2$ [56]. Further, no significant weight loss is observed up to 240 °C, after which the electrolyte degrades. This

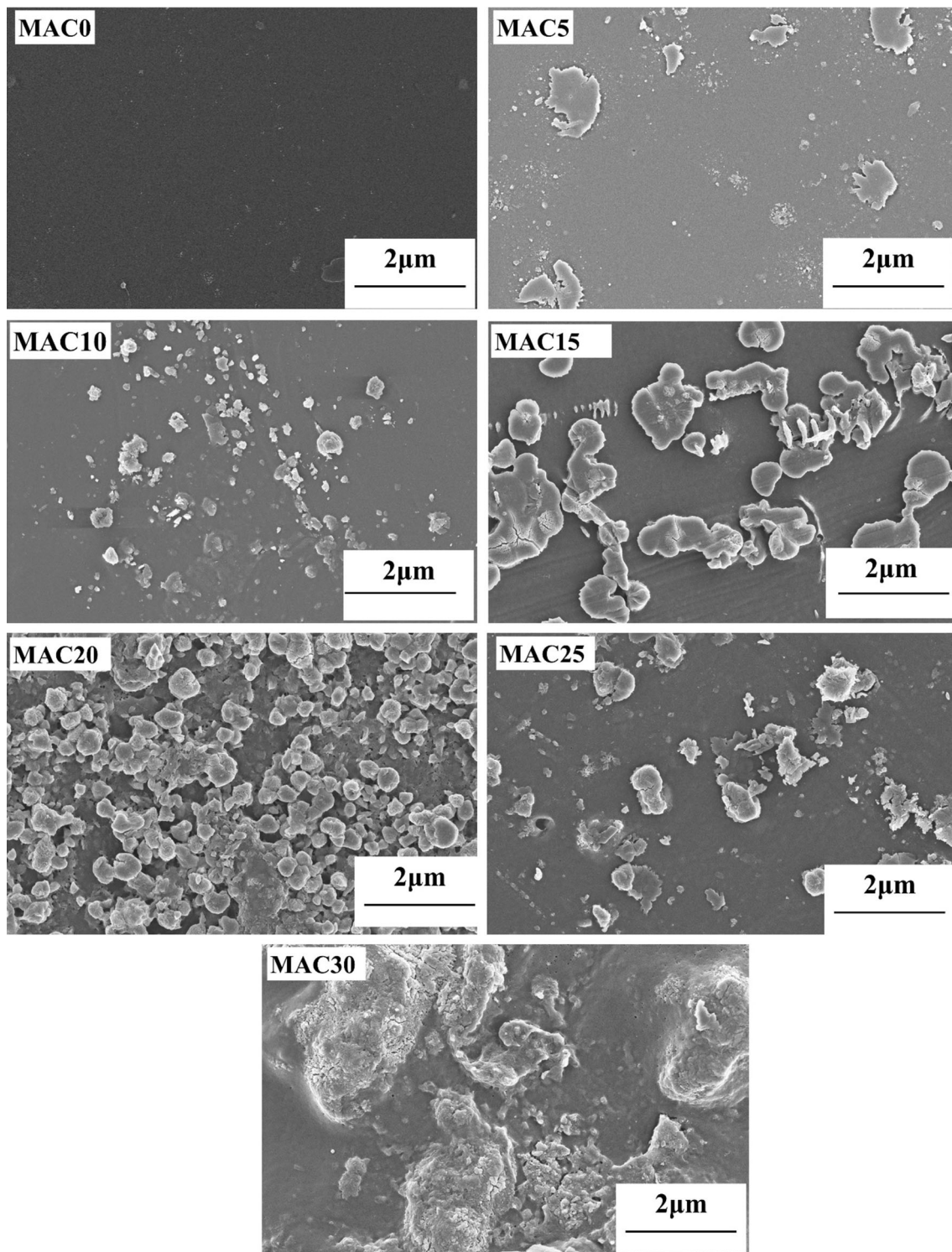


Figure 5 SEM micrographs of methyl cellulose-magnesium acetate polymer electrolytes.

accounts for the degradation of methyl cellulose polymer [56]. Compared with MAC0, the thermal stability of the polymer decreases with the inclusion

of salt, but the rate at which the degradation occurs slows down, which is evident from the TGA thermogram (Fig. 7).

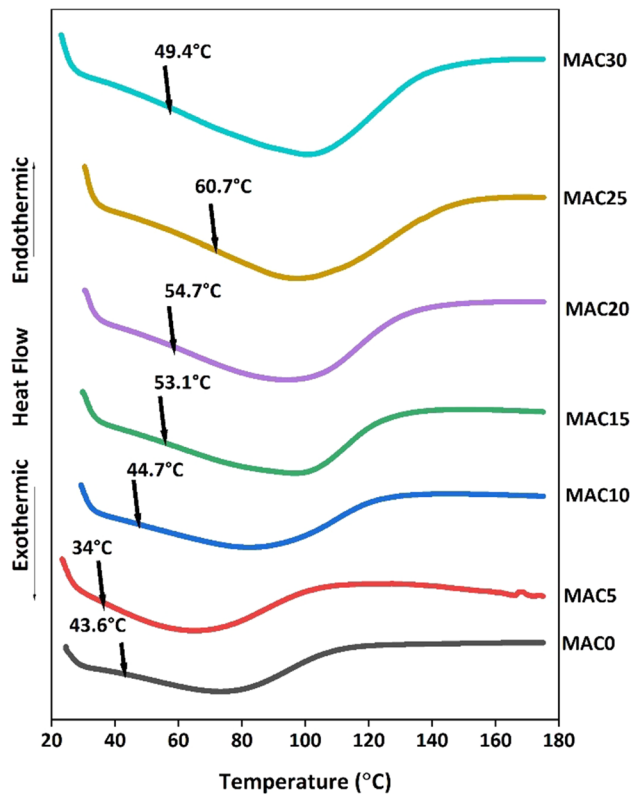


Figure 6 DSC thermogram of polymer electrolytes.

Table 5 Glass transition temperatures of prepared polymer electrolytes

Electrolyte	Glass transition temperature, T_g (in °C)
MAC0	43.6
MAC5	34.0
MAC10	44.7
MAC15	53.1
MAC20	54.7
MAC25	60.7
MAC30	49.4

Impedance analysis

Impedance spectra of polymer electrolytes enumerate the electrical properties of the electrolyte systems. Impedance analysis of the prepared polymer electrolytes was carried out, and a Cole–Cole plot was drawn with the real part of the impedance along the x-axis and the negative imaginary part of the impedance along the y-axis, as shown in Fig. 8. Generally, the Cole–Cole plot consists of a high-frequency semicircle and a low-frequency spike. In the present

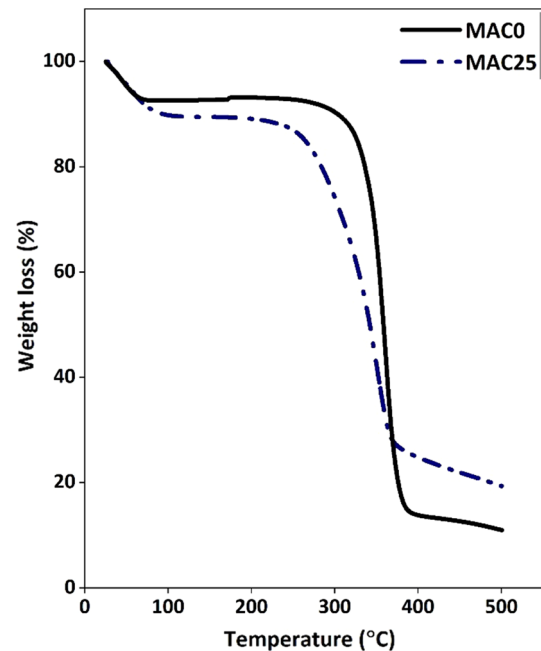


Figure 7 TGA thermogram of MAC0 and MAC25.

system, the Cole–Cole plot of pristine polymer film MAC0 and electrolyte films with low salt concentrations, i.e., MAC5 to MAC20, contain a depressed semicircle at a high-frequency region. In contrast, the Cole–Cole plot of MAC25 and MAC30 contains an inclined spike along with the depressed semicircle. A low-frequency inclined spike is due to the formation of a double layer due to the accumulation of charges at the electrode–electrolyte interface. The rapid increase in the dielectric constant and number density of electrolyte system with 25 wt% salt concentration, i.e., MAC25, further strengthens this nature. The depressed semicircle and inclined spikes in the Cole–Cole plot may be due to the inhomogeneities on the surface of the electrolyte films. Bulk resistance (R_b) of the films can be found by completing the semicircle to the x-axis [61, 62] DC ionic conductivity of the films was calculated using expression (3), and the values are tabulated in Table 6.

$$\sigma_{DC} = \frac{t}{R_b A} \quad (4)$$

From Table 3, enhancement in the ionic conductivity of the electrolyte can be observed despite the initial decrement with the incorporation of magnesium salt for MAC5. This decrement may be due to the electronic structure between $Mg(CH_3COO)_2$ and methyl cellulose polymer [54]. The reduction in the

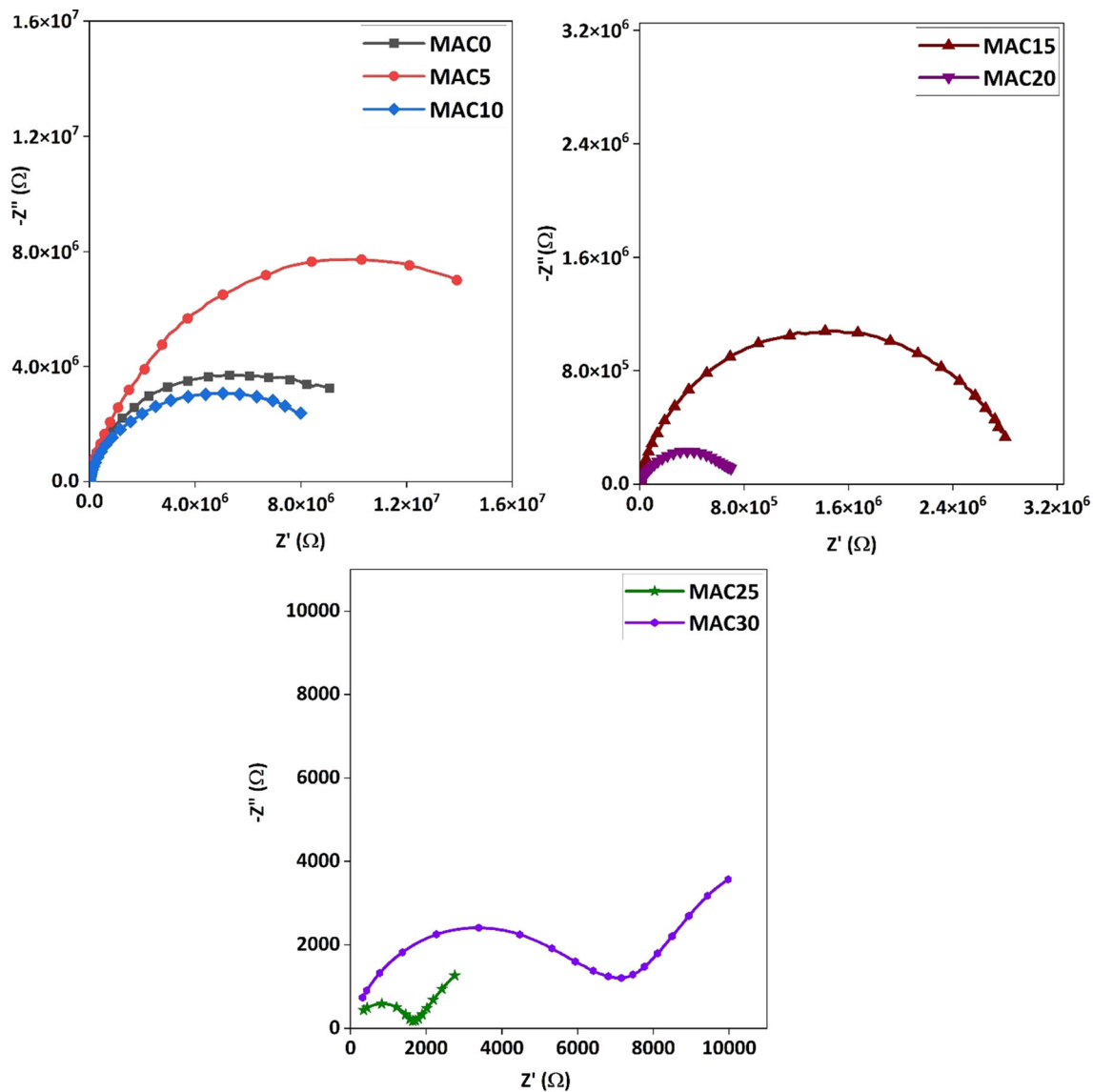


Figure 8 Cole–Cole plots of pristine and salt-doped polymer electrolyte systems.

Table 6 Bulk resistance, DC conductivities from Cole–Cole plot and obtained from the AC conductivity spectra

Electrolyte	Bulk resistance R_b (Ω)	Bulk conductivity σ_{DC} (S/cm)	DC conductivity from AC conductivity spectra at $\omega = 0$ (S/cm)
MAC0	6.33×10^6	8.05×10^{-9}	6.67×10^{-9}
MAC5	1.23×10^7	2.03×10^{-9}	1.85×10^{-9}
MAC10	8.85×10^6	3.93×10^{-9}	4.03×10^{-9}
MAC15	2.77×10^6	7.56×10^{-9}	7.36×10^{-9}
MAC20	6.69×10^5	4.45×10^{-8}	4.15×10^{-8}
MAC25	1.47×10^3	2.61×10^{-5}	2.45×10^{-5}
MAC30	5.85×10^3	4.25×10^{-6}	3.21×10^{-6}

bulk conductivity of MAC5 is in good agreement with XRD and SEM analysis. With the further inclusion of the salt, a linear increase in the ionic conductivity can be observed, which might be due to the availability of free ions since more and more salt gets dissociated with the increase in the salt content [39]. MAC25, an electrolyte system with 25wt% of magnesium acetate salt, is found to have the highest conductivity of 2.61×10^{-5} S/cm. With the addition of more salt, the ionic conductivity decreases. This is due to the recrystallization of the polymer matrix, as observed by XRD and SEM analysis.

Dielectric analysis

The complex permittivity of an electrolyte system can be expressed using the following expression:

$$\varepsilon^* = \varepsilon' - i\varepsilon'' \quad (5)$$

where ε' and ε'' represent the dielectric constant and dielectric loss of the system, respectively. These can be expressed using the following expressions [63]:

$$\varepsilon' = \frac{C_p d}{A \varepsilon_0} \quad \text{and} \quad \varepsilon'' = \varepsilon' \times \tan \delta \quad (6)$$

where C_p represents the system's capacitance, d is the thickness, A is the electrolyte area, $\tan \delta$ represents the loss factor of the system, and ε_0 (8.85×10^{-12} F/m) is the permittivity of free space.

The system's dielectric constant (ε') represents the amount of dipoles aligned at the electrode–electrolyte

interface due to the polarization effects such as deformational and relaxation polarization [64]. The variation of the dielectric constant as a function of logarithmic angular frequency ($\log \omega$) is shown in Fig. 9. It can be observed that ε' decreases with an increase in the frequency for all the electrolyte systems and attain constant at a higher frequency. This variation is due to several reasons. When an electric field is applied to an electrolyte sandwiched between blocking electrodes, the system's induced and permanent dipoles migrate along the field and pile up at the blocking electrodes, causing the system to polarize [65]. At low frequency, the presence of ion pairs results in the long-range frequency, which is attributed to the higher value of ε' at low frequency. As the frequency increases, the periodic reversal of the field increases. However, the heavy dipoles fail along the direction of the periodic reversal of the field, resulting in the decrease in ε' . At higher frequency, the field direction reverses faster than the alignment of dipoles. Thus, the dielectric constant becomes constant at the higher frequency of the field since the field's periodic reversal inhibits ion diffusion [64, 65].

Dielectric loss (ε'') of the electrolyte system is the energy dissipated due to the movement of dipoles along with the matrix upon the application of electric field [64]. Figure 10 gives the variation of dielectric loss as the function of $\log \omega$. Variation of ε'' follows a similar trend as that of ε' . With the increase in frequency, dipoles undergo continuous acceleration and

Figure 9 Variation of ε' versus $\log \omega$.

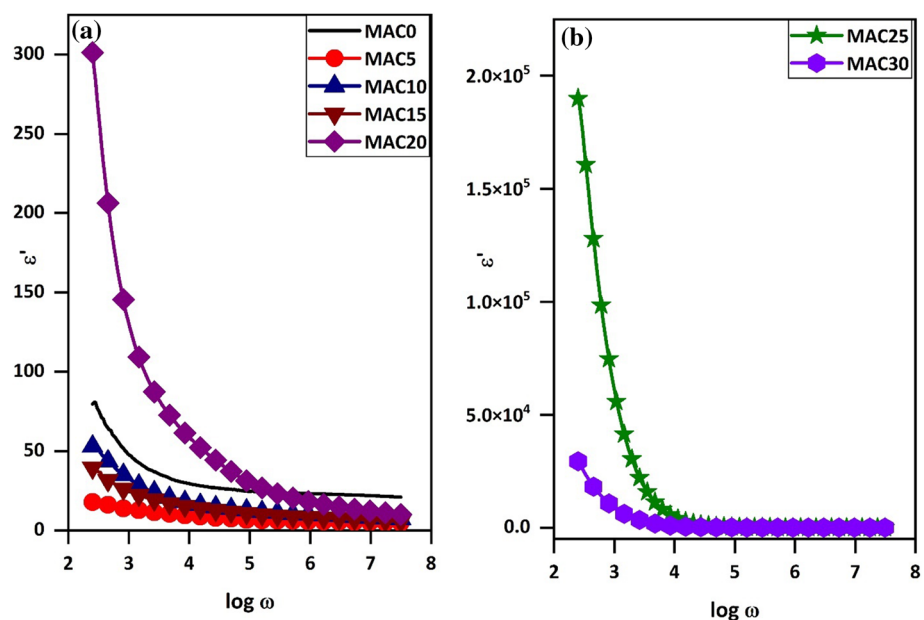


Figure 10 Variation of ϵ'' versus $\log \omega$.

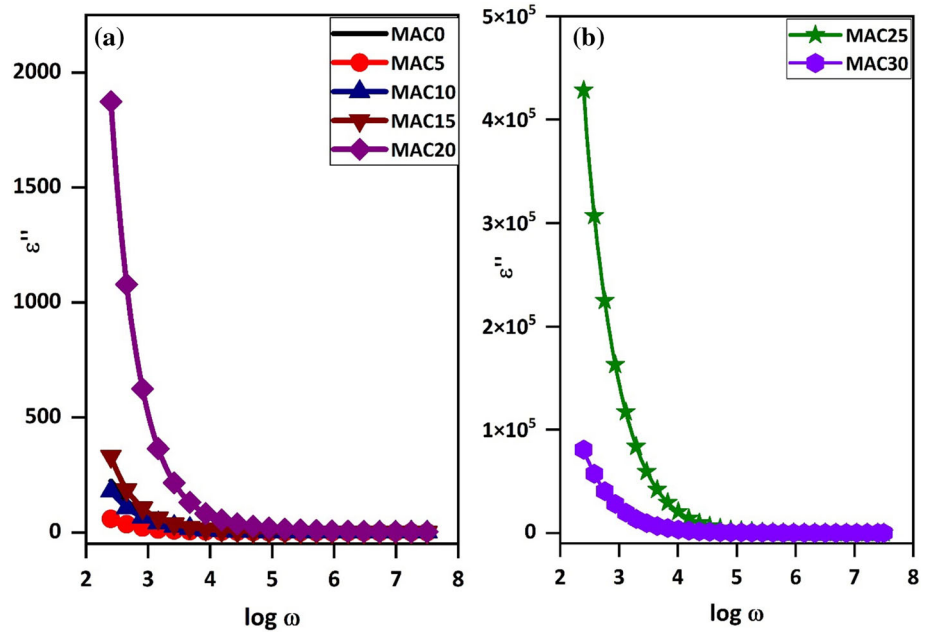
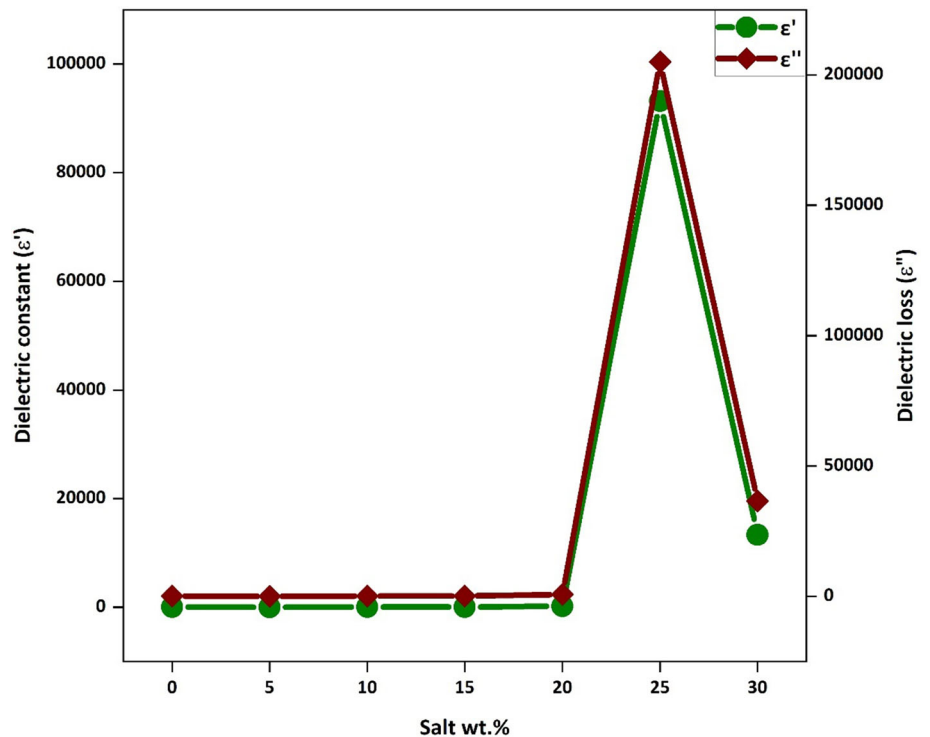


Figure 11 Variation of dielectric constant and dielectric loss with salt concentration at 100 Hz.



deceleration, resulting in the dissipation of dielectric loss as heat energy. Thus, dielectric loss decreases with the increase in frequency.

Variation of dielectric constant and dielectric loss with salt concentration at a frequency of 100 Hz is shown in Fig. 11, and values are tabulated in Table 7. An initial decrease in both ϵ' and ϵ'' can be observed

with the incorporation of magnesium salt. The literature shows that the dielectric constant linearly depends on molecular polarization and free volume [66, 67]. From DSC analysis, a decrement in the glass transition temperature of the polymer matrix with the incorporation of salt can be observed for MAC5, indicating a slight decrease in the free volume of the

Table 7 Variation of dielectric constant and dielectric loss with salt concentration at 100 Hz

Electrolyte	Dielectric constant (ϵ')	Dielectric loss (ϵ'')
MAC0	56.8	103.5
MAC5	15.0	25.8
MAC10	38.1	80.2
MAC15	28.1	133.8
MAC20	165.8	776.4
MAC25	93,227.8	204,952.6
MAC30	13,354.4	36,493.5

matrix [67]. Thus, the dielectric constant decreases slightly with the incorporation of salt and then linearly increases with the addition of the salt. This might be due to the increase in the free volume of the matrix and chain flexibility, as observed from XRD and DSC analysis [64]. Similar variation can be observed for dielectric loss of the electrolyte systems. The initial decrease might be due to the slight reduction in the matrix's free volume. However, dielectric loss increases linearly with the salt concentration despite the initial decrease. Both ϵ' and ϵ'' become maximum for MAC25, the highest conducting system. The following expression can relate the dielectric constant and number density of the polymer electrolytes:

$$n = n_0 \exp\left(\frac{-U}{\epsilon' k_B T}\right)$$

where n_0 is a pre-exponential factor, U is the dissociation energy, k_B is the Boltzmann constant, ϵ' represents the dielectric constant of the system, and T is the temperature. The equation represents the direct correlation between the dielectric constant and number density, which is further related to ionic conductivity ($\sigma = n\mu e$). It can be observed that number density and ionic conductivity attain maximum for MAC25 and then decreases with further inclusion of the salt, which can be accounted for the recrystallization of polymer matrix corresponding to the presence of ion aggregates in the system as observed from SEM micrographs. Due to these factors, MAC25 shows maximum dielectric constant compared to other systems. With further inclusion of the salt, dielectric constant and dielectric loss decrease since recrystallization occurs, as observed from XRD and SEM studies.

AC conductivity analysis

AC conductivity of the electrolyte systems was calculated using equation [65]:

$$\sigma_{AC} = \omega \epsilon_0 \epsilon'' \quad (7)$$

where ω is the angular frequency of the applied field, ϵ_0 represents the permittivity of the free space (8.85×10^{-12} F/m), and ϵ'' is the dielectric loss of the electrolyte system. The AC conductivity spectra of the prepared polymer electrolytes are found to obey Universal Jonscher's power law given by expression [63]:

$$\sigma_{AC}(\omega) = \sigma_{DC} + A\omega^n \quad (8)$$

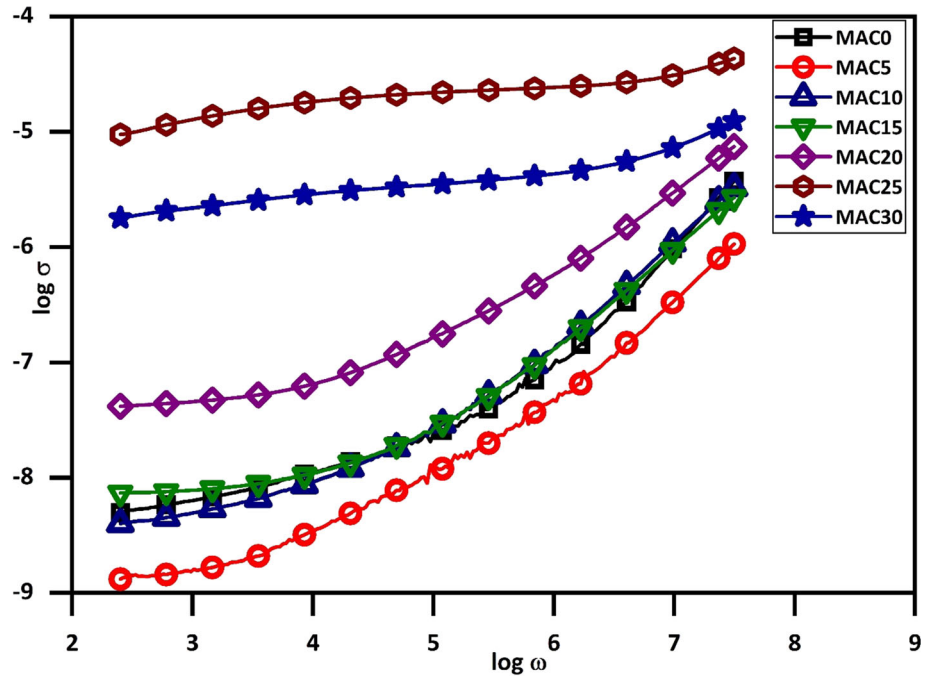
where ω is the angular frequency, A is a temperature-dependent parameter, and n is the frequency exponent, which takes values between 0 and 1 [68, 69], σ_{AC} and σ_{DC} are AC conductivity, and DC conductivity of the system, respectively.

AC conductivity spectra of pristine and salt-doped polymer electrolyte films against $\log \omega$ are shown in Fig. 12. Generally, the spectra contain three different regions: low-frequency dispersion region, mid-frequency plateau region, and high-frequency dispersion region. The low-frequency dispersion region may be due to the accumulation of charges at the blocking electrodes forming a space-charge layer resulting in electrode polarization [70]. The intermediate frequency-independent plateau region results from long-range ion diffusion. In contrast, the high-frequency dispersion region is due to the short-range diffusion of ions associated with the AC conductivity [65]. DC conductivity of the electrolyte systems can be extracted from the mid-frequency plateau region, and the values are tabulated in Table 6. These values agree with the ones calculated from the Cole–Cole plot.

Transport parameter analysis

The conduction mechanism in polymer electrolyte films is elucidated by transport parameters such as number density n , mobility μ , and diffusion coefficient D of mobile ions. These parameters can be found by employing different techniques. According to the literature, the FTIR analysis technique efficiently finds the transport parameters [71, 72]. The region between 1350 and 1600 cm^{-1} of the FTIR spectra has been deconvoluted where anion active peaks were found [73, 74]. Deconvolution was carried

Figure 12 AC conductivity spectra of polymer electrolytes.



out employing the Gaussian function with the help of Origin software, and the graphs are shown in Fig. 13. Among the deconvoluted peaks, peaks around 1414 cm^{-1} and between $1550\text{--}1580\text{ cm}^{-1}$ correspond to the free ions of the magnesium salt, and the peak corresponding to the contact ions exists around 1454 cm^{-1} [60, 75]. The peak around 1375 cm^{-1} accounts for the C-H bending mode of methyl cellulose [39]. The percentage of free ions can be found using Eq. (8) [13], and the values are tabulated in Table 8.

$$\% \text{ of free ions} = \frac{A_f}{A_f + A_c} \times 100\% \tag{9}$$

where A_f and A_c correspond to the area under the peaks corresponding to free ions and contact ions, and transport parameters were calculated using the following equations:

$$n = \frac{M \times N_A}{V_{\text{TOTAL}}} \times \% \text{ of free ions} \tag{10}$$

$$\mu = \frac{\sigma_{\text{DC}}}{ne} \tag{11}$$

$$D = \frac{\mu k_B T}{e} \tag{12}$$

where M is the number of moles of salt doped into the system, N_A is the Avogadro number ($6.022 \times 10^{23}\text{ mol}^{-1}$), V_{TOTAL} is the total volume of the electrolyte, σ_{DC} is the bulk conductivity, e

represents the charge of the electron ($1.6 \times 10^{-19}\text{ C}$), k_B is the Boltzmann constant ($1.38 \times 10^{-23}\text{ J/K}$), and T is the absolute temperature of the system. The values are tabulated in Table 8.

Variation of these transport properties with the salt concentration is shown in Fig. 14. From the figure, a linear increase in the transport properties can be observed. According to free volume theory, free volume availability facilitates ions' conduction in the electrolyte system, along with other terms [76]. A decrease in the matrix's free volume is evident from the increase in the glass transition temperature from the DSC analysis, resulting in the creation of transient crosslinks that inhibit the movement of polymer segments. Although free volume decreases as salt concentration increases, this decrease is offset by an increase in number density, resulting in a linear increase in the electrolyte system's ionic conductivity [76]. As observed from XRD studies, an increase in the mobility of mobile ions with the salt concentration could be attributed to the increase in the amorphous phase of the polymer matrix [73]. Thus, mobility increases with the increase in salt concentration. A similar explanation can be given for the increase in the diffusion coefficient, D . MAC25 has the highest number density n , mobility μ , and diffusion coefficient D , resulting in the maximum ionic conductivity. The cumulative effect of n , μ , and D result in the enhancement of the ionic conductivity

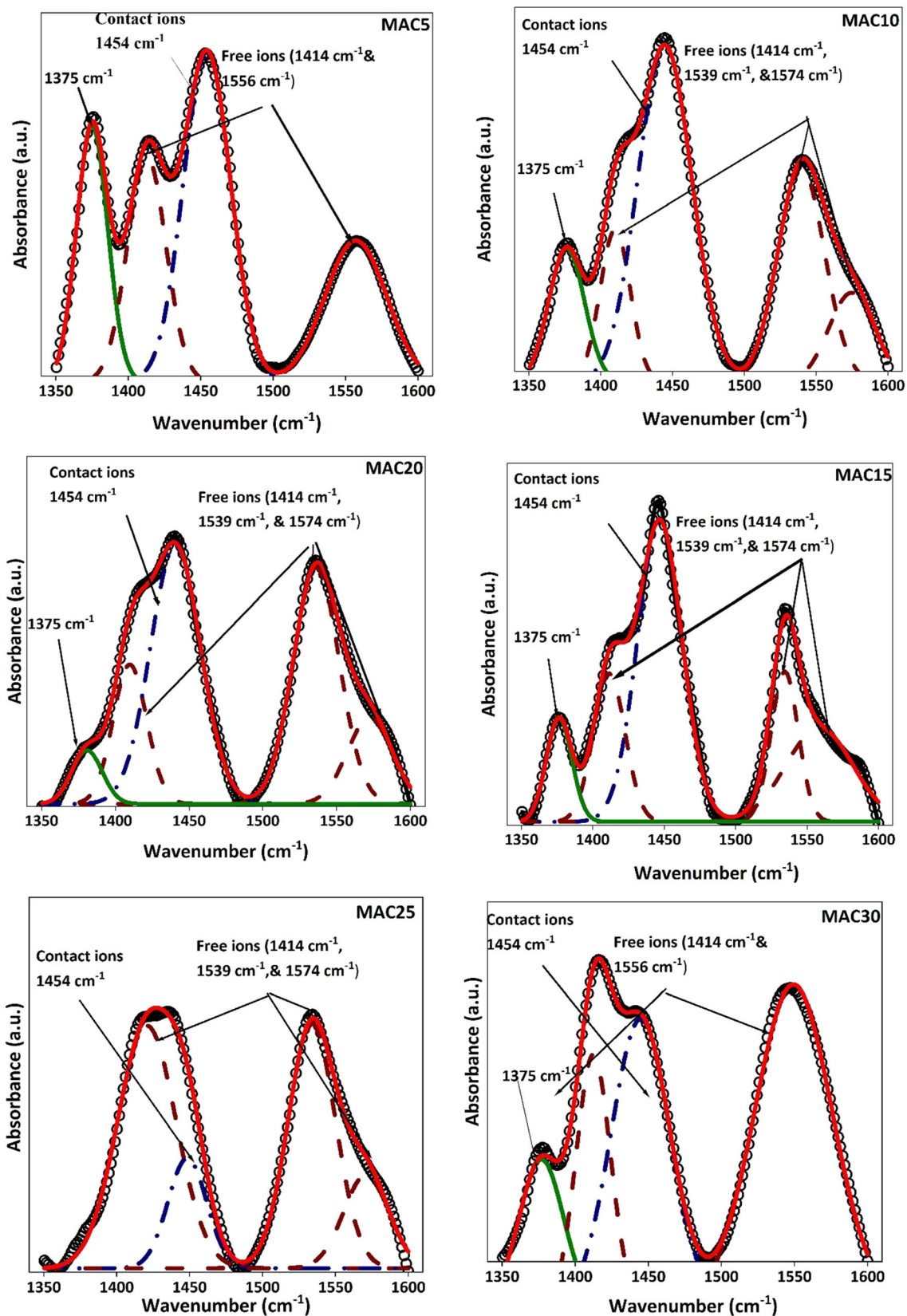
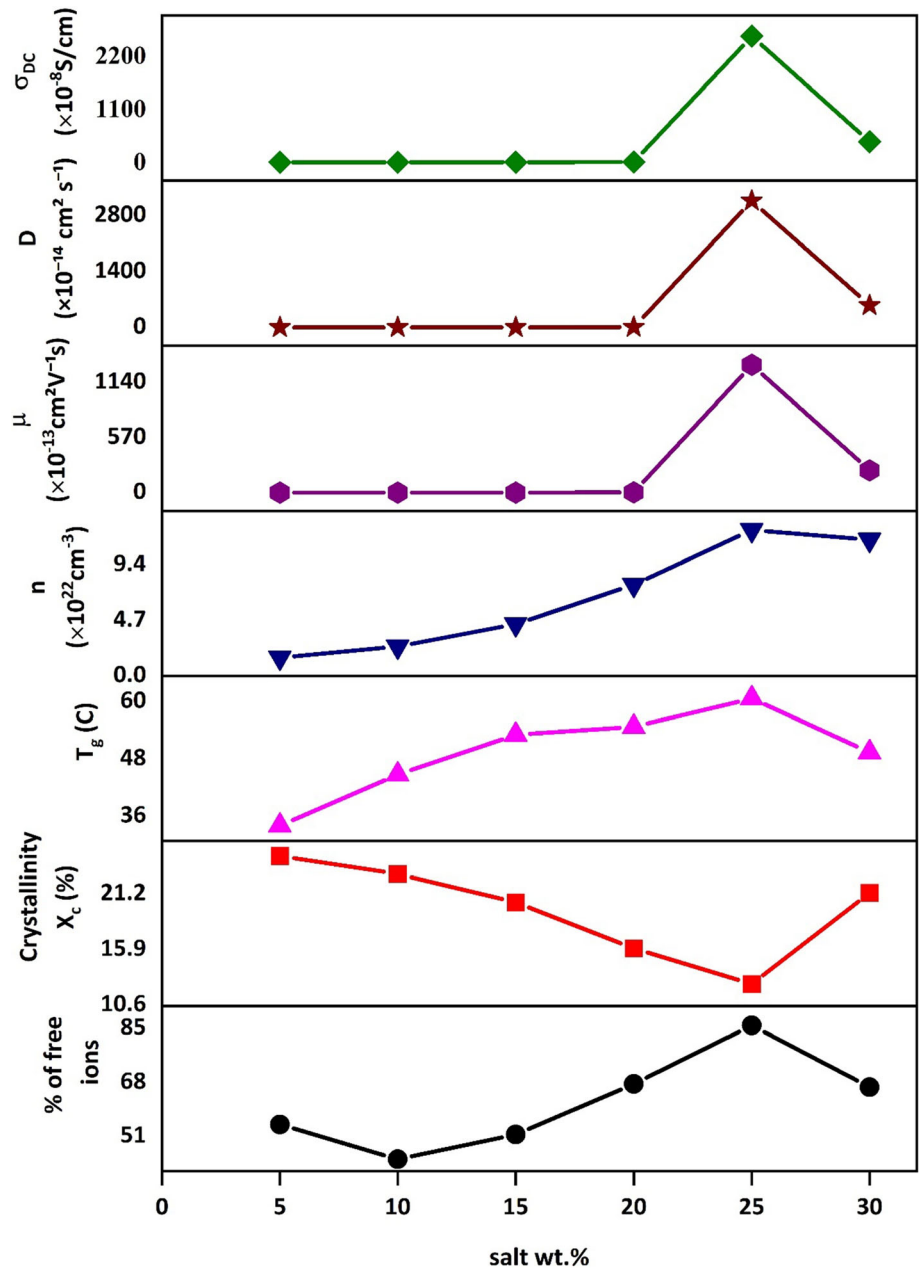


Figure 13 Deconvolution of FTIR spectra in the range between 1350 and 1600 cm^{-1} .

Table 8 % of free ions, number density n , mobility μ , and diffusion coefficient D of salt-doped polymer electrolytes

Electrolyte	% of free ions	Number density n ($\times 10^{22} \text{ cm}^{-3}$)	Mobility μ ($\times 10^{-12} \text{ cm}^2 \text{ V}^{-1} \text{ s}$)	Diffusion coefficient D ($\times 10^{-14} \text{ cm}^2 \text{ s}^{-1}$)	DC conductivity σ_{DC}
MAC5	54.7	1.55	0.83	1.97	2.03×10^{-9}
MAC10	43.8	2.48	0.99	2.37	3.93×10^{-9}
MAC15	51.6	4.40	1.07	2.57	7.56×10^{-9}
MAC20	67.5	7.72	3.60	8.64	4.45×10^{-8}
MAC25	85.9	12.34	1323.04	3172.33	2.61×10^{-5}
MAC30	66.5	11.51	230.82	553.45	4.25×10^{-6}

Figure 14 Variation of transport parameters with the salt concentration.



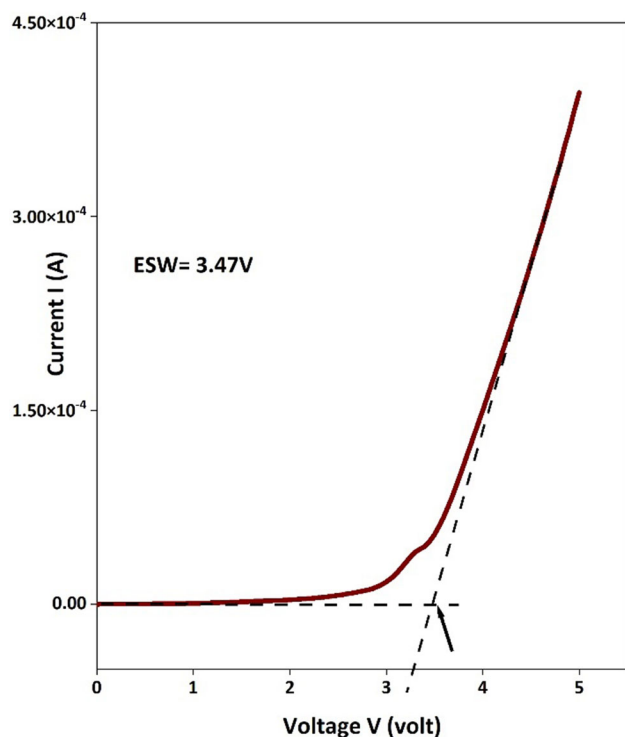


Figure 15 *I*–*V* characteristics of MAC25.

of the matrix [77]. With the further insertion of the salt, for MAC30, all three transport parameters n , μ , and D decrease due to the polymer matrix's recrystallization, which the XRD and SEM analysis indicate.

Electrochemical stability window

The electrochemical/voltage stability window of the highest conducting polymer electrolyte was found from the *I*–*V* characteristics of the film. *I*–*V* characteristics of MAC25 is given in Fig. 15. ESW of the film was found by extrapolating the linear portion into the *x*-axis. The value of ESW of MAC25 was 3.47 V, which denotes the suitability of the electrolyte in energy storage devices [8].

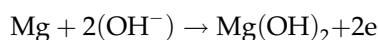
Fabrication of primary battery

A magnesium ion-conducting primary battery was fabricated using the highest conducting polymer electrolyte film. The cathode was prepared by grinding the mixture of MnO_2 , graphite, and MAC25 in a ratio of 3:1:1, and magnesium metal powder was used to prepare the anode. The cathode and anode mixtures were made into pellets using the pellet pressing machine under 5 ton pressure. MAC25 film

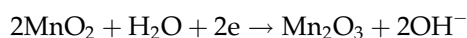
was sandwiched between the anode and cathode and open-circuit potential and discharge characteristics of the battery across a 100k Ω resistor for 24 h, and the characteristics are shown in Fig. 16. Also, the cell parameters are given in Table 9.

The variation of open-circuit potential as a function of time is given in Fig. 16a. Initially, the battery showed an open-circuit potential of 2.013 V, which decreased with time and attained a constant value after 1500 min. This decrease may be due to the reaction across the cell components, which can be shown below [20]:

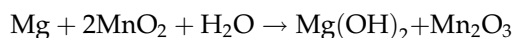
At the anode:



At the cathode:



Thus, the overall reaction would be:



Methyl cellulose contains hydroxy groups, which act as a source of hydroxyl ions [20].

Figure 16b shows the discharge characteristics of the prepared battery across an external load of 100 k Ω . A decrease in the open-circuit potential can be observed after connecting to the external load. This might be due to the polarization effect at the electrode–electrolyte interface [20]. Initially, a potential of 1.343 V was observed, which decreased gradually with time. The characteristics of the battery was studied for 26 h, and the battery has drawn a short-circuit current of 2.5 mA discharging from 1.343 to 0.559 V. Table 10 lists the comparison between the present work and other works found in the literature. Table 10 indicates the suitability of the prepared polymer electrolyte system to be an efficient candidate for energy storage applications with good OCV value and energy density which is comparable with the data found in the literature. In addition, the prepared battery's performance has been studied by glowing a green LED using two primary batteries connected in series as shown in Fig. 17. The series combination of two primary batteries produced a potential difference of 3.78 V. The combination of the batteries could glow the LED for about 49 h.

Figure 16 **a** Open-circuit potential of the prepared primary battery, **b** discharge characteristics.

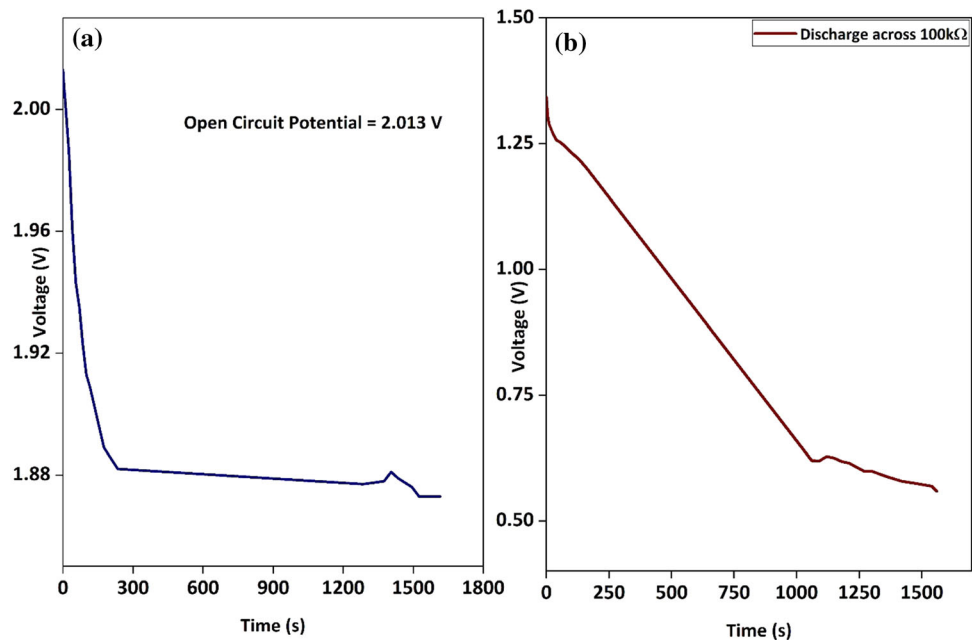


Table 9 Cell parameters across 100kΩ resistor

Cell parameters	Measured values of discharge across 100kΩ
Cell area (cm ²)	1.13
Cell weight (g)	1.478
Effective cell diameter (cm)	1.2
Cell thickness (cm)	0.7
Open-circuit voltage, OCV (in V)	2.013
Current drawn (mA)	2.5
Discharge capacity (mA/h)	2.5
Current density (m/cm ²)	2.21
Energy density (Wh/kg)	3.405
Power density (W/kg)	3.41

Table 10 Comparison of OCV and energy density values of present work with other works found in the literature

Electrolyte system	OCV (V)	Energy density (Wh/kg)
poly(VdCl-co-AN-co-MMA): MgCl ₂ (70:30) [78]	2.18	NA
PVA: Mg(CH ₃ COO) ₂ (80:20) [21]	1.84	1.940
PVA: Mg(NO ₃) ₂ (70:30) [24]	1.85	2.288
PVP: MgCl ₂ (85:15) [79]	2.01	270.200
PEG: Mg(CH ₃ COO) ₂ (80:20) [25]	1.84	1.681
Methyl cellulose: Mg(CH ₃ COO) ₂ (75:25) [PRESENT WORK]	2.013	3.405

Conclusion

Biodegradable solid polymer electrolyte films based on methyl cellulose and magnesium acetate tetrahydrate were prepared using the solution casting

technique. The films’ structural, thermal, and electrical properties were analyzed, and few observations can be made. The incorporation of the salt into the matrix enhanced the amorphousness of the polymer matrix, thereby facilitating the movements of the

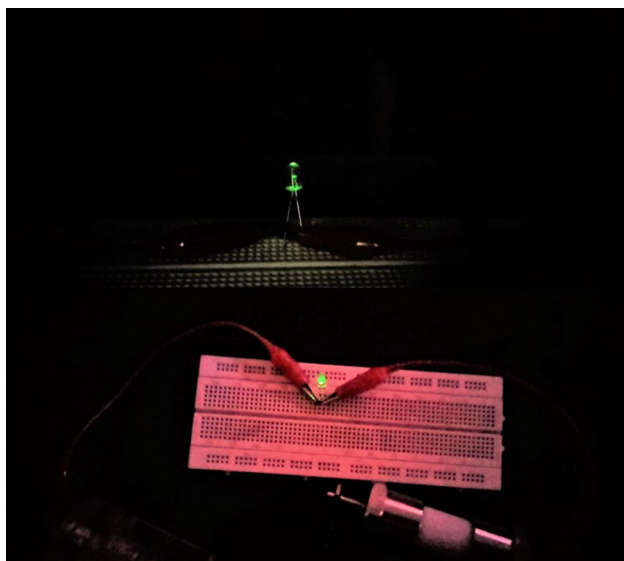


Figure 17 LED glowing using two primary magnesium ion conducting batteries.

polymer segments. Complexation of the salt with the polymer matrix is evident from FTIR and SEM analysis. With the addition of salt, the electrical conductivity of the films was enhanced, and MAC25 was found to exhibit the highest conductivity of 2.61×10^{-5} S/cm. The unusual variation of dielectric properties with salt concentration can be attributed to the initial decrease in the matrix's free volume with salt incorporation, as observed in XRD and DSC studies. A primary battery was fabricated employing MAC25, and its open-circuit potential and discharge characteristics were studied. Despite the low conductivity compared to other polymer electrolyte systems, the proposed electrolyte system represents good structural and electrical properties and exhibits excellent thermal stability.

Acknowledgements

The author Jayalakshmi Koliyoor gratefully acknowledge the financial support from the Manipal Academy of Higher Education in the form of TMA Pai PhD fellowship.

Funding

Open access funding provided by Manipal Academy of Higher Education, Manipal.

Declarations

Conflict of interest The authors declare that there are no conflicts of interest to disclose.

Ethical approval This study was carried out following all ethical standards; neither human participants nor animals were used during the study.

Open Access This article is licensed under a Creative Commons Attribution 4.0 International License, which permits use, sharing, adaptation, distribution and reproduction in any medium or format, as long as you give appropriate credit to the original author(s) and the source, provide a link to the Creative Commons licence, and indicate if changes were made. The images or other third party material in this article are included in the article's Creative Commons licence, unless indicated otherwise in a credit line to the material. If material is not included in the article's Creative Commons licence and your intended use is not permitted by statutory regulation or exceeds the permitted use, you will need to obtain permission directly from the copyright holder. To view a copy of this licence, visit <http://creativecommons.org/licenses/by/4.0/>.

References

- [1] Fan L, Yanyao Hu, Rao AM, Zhao J, Wang C, Bingan Lu (2021) Prospects of electrode materials and electrolytes for practical potassium-based batteries. *Small Methods* 5:2101131. <https://doi.org/10.1002/smt.202101131>
- [2] Fan X, Wang C (2021) High-voltage liquid electrolytes for Li batteries: progress and perspectives. *Chem Soc Rev* 50:10486–10566. <https://doi.org/10.1039/D1CS00450F>
- [3] Liu S, Zhang R, Mao J, Zhao Y, Cai Q, Guo Z (2022) From room temperature to harsh temperature applications: fundamentals and perspectives on electrolytes in zinc metal batteries. *Sci Adv* 8:5097. <https://doi.org/10.1126/sciadv.abn5097>
- [4] Arya A, Sharma AL (2019) Electrolyte for energy storage/conversion (Li^+ , Na^+ , Mg^{2+}) devices based on PVC and their associated polymer: a comprehensive review. *J Solid State Electrochem* 23:997–1059. <https://doi.org/10.1007/s10008-019-04203-x>
- [5] Aziz SB, Woo TJ, Kadir MFZ, Ahmed HM (2018) A conceptual review on polymer electrolytes and ion transport models. *J Sci Adv Mater Dev* 3:1–17. <https://doi.org/10.16/j.jsamd.2018.01.002>

- [6] Sudhakar YN, Selvakumar M, Bhat DK (2018) Biopolymer electrolytes. Elsevier, Cambridge
- [7] Alves RD et al (2013) Study and characterization of a novel polymer electrolyte based on agar doped with magnesium triflate. *Mol Cryst Liq Cryst* 570:1–11. <https://doi.org/10.1080/15421406.2012.703041>
- [8] Mahalakshmi M, Selvanayagam S, Selvasekarapandian S, Chandra MVL, Sangeetha P, Manjuladevi R (2020) Magnesium ion-conducting solid polymer electrolyte based on cellulose acetate with magnesium nitrate ($\text{Mg}(\text{NO}_3)_2 \cdot 6\text{H}_2\text{O}$) for electrochemical studies. *Ionics* 36:4553–4565. <https://doi.org/10.1007/s11581-020-03615-4>
- [9] Wu K et al (2020) Recent advances in polymer electrolytes for zinc ion batteries: mechanisms, properties, and perspectives. *Adv Energy Mater* 10:1903977. <https://doi.org/10.1002/AENM.201903977>
- [10] Bergfelt A, Lacey MJ, Hedman J, Sångeland C, Brandell D, Bowden T (2018) ϵ -Caprolactone-based solid polymer electrolytes for lithium-ion batteries: synthesis, electrochemical characterization and mechanical stabilization by block copolymerization. *RSC Adv* 8:16716–16725. <https://doi.org/10.1039/C8RA00377G>
- [11] Fullerton-Shirey SK, Maranas JK (2009) Effect of LiClO_4 on the structure and mobility of PEO-based solid polymer electrolytes. *Macromolecules* 42:2142–2156. <https://doi.org/10.1021/ma802502u>
- [12] Shetty SK, Ismayil, Shetty G (2020) Enhancement of electrical and optical properties of sodium bromide doped carboxymethyl cellulose biopolymer electrolyte films. *J Macromol Sci Part B* 59:235–247. <https://doi.org/10.1080/00222348.2020.1711585>
- [13] Shetty SK, Ismayil A, Hegde S, Ravindrachary V, Sanjeev G, Bhajantri RF, Masti SP (2021) Dielectric relaxations and ion transport study of $\text{NaCMC}:\text{NaNO}_3$ solid polymer electrolyte films. *Ionics* 27:2505–2527. <https://doi.org/10.1007/s11581-021-04023-y>
- [14] Cyriac V, Ismayil A, Noor IM, Mishra K, Chavan C, Bhajantri RF, Masto SP (2022) Ionic conductivity enhancement of PVA: carboxymethyl cellulose poly-blend electrolyte films through the doping of NaI salt. *Cellulose* 29:3271–3291. <https://doi.org/10.1007/s10570-022-04483-z>
- [15] Zhou D, Shanmukaraj D, Tkacheva A, Armand M, Wang G (2019) Polymer electrolytes for lithium-based batteries: advances and prospects. *Chem* 5:2326–2352. <https://doi.org/10.1016/J.CHEMPR.2019.05.009>
- [16] Arya A, Sharma AL (2020) A glimpse on all-solid-state Li-ion battery (ASSLIB) performance based on novel solid polymer electrolytes: a topical review. *J Mater Sci* 55:6242–6304. <https://doi.org/10.1007/s10853-020-04434-8>
- [17] Park B, Schaefer JL (2020) Review—polymer electrolytes for magnesium batteries: forging away from analogs of lithium polymer electrolytes and towards the rechargeable magnesium metal polymer battery. *J Electrochem Soc* 167:070545. <https://doi.org/10.1149/1945-7111/ab7c71>
- [18] Deivanayagam R, Cheng M, Wang M, Vasudevan V, Fro-roozan T, Medhkar NV, Yassar RS (2019) Composite polymer electrolyte for highly cyclable room-temperature solid-state magnesium batteries. *ACS Appl Energy Mater* 2:7980–7990. <https://doi.org/10.1021/acsaem.9b01455>
- [19] Deivanayagam R, Ingram BJ, Shahbazian-Yassar R (2019) Progress in development of electrolytes for magnesium batteries. *Energy Storage Mater* 21:136–153. <https://doi.org/10.1016/J.ENSMS.2019.05.028>
- [20] Manjuladevi R, Thamilselvan M, Selvasekarapandian S, Christopher Selvin P, Mangalam R, Monisha S (2018) Preparation and characterization of blend polymer electrolyte film based on poly(vinyl alcohol)-poly(acrylonitrile)/ MgCl_2 for energy storage devices. *Ionics* 24:1083–1095. <https://doi.org/10.1007/s11581-017-2273-9>
- [21] Polu AR, Kumar R (2013) Ionic conductivity and discharge characteristic studies of $\text{PVA-Mg}(\text{CH}_3\text{COO})_2$ solid polymer electrolytes. *Int J Polym Mater Polym Biomater* 62:76–80. <https://doi.org/10.1080/00914037.2012.664211>
- [22] Shanmuga Priya S, Karthika M, Selvasekarapandian S, Manjuladevi R (2018) Preparation and characterization of polymer electrolyte based on biopolymer I-Carrageenan with magnesium nitrate. *Solid State Ionics* 327:136–149. <https://doi.org/10.1016/j.ssi.2018.10.031>
- [23] Shanmuga Priya S, Karthika M, Selvasekarapandian S, Manjuladevi R, Monisha S (2018) Study of biopolymer I-carrageenan with magnesium perchlorate. *Ionics* 24:3861–3875. <https://doi.org/10.1007/s11581-018-2535-1>
- [24] Polu AR, Kumar R (2013) Preparation and characterization of PVA based solid polymer electrolytes for electrochemical cell applications. *Chin J Polym Sci* 31:641–648. <https://doi.org/10.1007/s10118-013-1246-3>
- [25] Reddy Polu A, Kumar R (2012) Ion-conducting polymer electrolyte based on poly (ethylene glycol) complexed with $\text{Mg}(\text{CH}_3\text{COO})_2$ -application as an electrochemical cell. *E J Chem* 9:869–874
- [26] Kiruthika S, Malathi M, Selvasekarapandian S, Tamilarasan K, Maheshwari T (2020) Conducting biopolymer electrolyte based on pectin with magnesium chloride salt for magnesium battery application. *Polym Bull* 77:6299–6317. <https://doi.org/10.1007/s00289-019-03071-9>
- [27] Rani NS, Sannappa J, Demappa T, Mahadevaiah (2014) Structural, thermal, and electrical studies of sodium iodide (NaI)-doped hydroxypropyl methylcellulose (HPMC)

- polymer electrolyte films. *Ionics (Kiel)* 20:201–207. <https://doi.org/10.1007/S11581-013-0952-8/TABLES/4>
- [28] Hamsan MH, Aziz SB, Shukur MF, Kadir MFZ (2019) Protonic cell performance employing electrolytes based on plasticized methylcellulose-potato starch-NH₄NO₃. *Ionics (Kiel)* 25:559–572. <https://doi.org/10.1007/S11581-018-2827-5/FIGURES/13>
- [29] Aziz SB, Hamsan MH, Abdullah RM, Kadir MFZ (2019) A promising polymer blend electrolytes based on chitosan: methyl cellulose for EDLC application with high specific capacitance and energy density. *Molecules* 24:16724–16736. <https://doi.org/10.3390/molecules24132503>
- [30] Hamsan MH et al (2020) Solid-state double layer capacitors and protonic cell fabricated with Dextran from *Leuconostoc mesenteroides* based green polymer electrolyte. *Mater Chem Phys* 241:122290. <https://doi.org/10.1016/J.MATCHEMPHYS.2019.122290>
- [31] Bharti V, Singh PK, Sharm JP (2021) Development of polymer electrolyte membranes based on biodegradable polymer. *Mater Today Proc* 34:856–862. <https://doi.org/10.1016/J.MATPR.2020.06.463>
- [32] J. Brady, T. Drig, P. I. Lee, and J. X. Li (2017) Polymer properties and characterization. In: *Developing solid oral dosage forms: pharmaceutical theory and practice: Second Edition* 181–223. <https://doi.org/10.1016/B978-0-12-802447-8.00007-8>.
- [33] Shuhaimi NEA, Teo LP, Majid SR, Arof AK (2010) Transport studies of NH₄NO₃ doped methyl cellulose electrolyte. *Synth Met* 160:1040–1044. <https://doi.org/10.1016/j.synthmet.2010.02.023>
- [34] Nasatto PL, Pignon F, Silveira JLM, Duarte MER, Nosedo MD, Rinaudo M (2015) Methylcellulose, a cellulose derivative with original physical properties and extended applications. *Polymers* 7:777–803. <https://doi.org/10.3390/POLYM7050777>
- [35] Thirumala S, Gimble JM, Devireddy RV (2013) Methylcellulose based thermally reversible hydrogel system for tissue engineering applications. *Cells* 2:460–475. <https://doi.org/10.3390/CELLS2030460>
- [36] Abdullah OG, Aziz BK, Aziz SB, Suhail MH (2018) Surfaces modification of methylcellulose: cobalt nitrate polymer electrolyte by sulfurated hydrogen gas treatment. *J Appl Polym Sci* 135:46676–46683. <https://doi.org/10.1002/app.46676>
- [37] Nurhaziqah AMS, Afiqah IQ, Aziz MFHA, Aziz NAN, Hasiah S (2018) Optical, structural and electrical studies of biopolymer electrolytes based on methylcellulose doped with Ca(NO₃)₂. In: *IOP conference series: materials science and engineering* 440:012034. <https://doi.org/10.1088/1757-899X/440/1/012034>
- [38] Yusof YM, Kadir MFZ (2016) Electrochemical characterizations and the effect of glycerol in biopolymer electrolytes based on methylcellulose-potato starch blend. *Mol Cryst Liq Cryst* 627:220–233. <https://doi.org/10.1080/15421406.2015.1137115>
- [39] Koliyoor J, Ismayil S, Hegde RV, Sanjeev G (2022) Novel solid biopolymer electrolyte based on methyl cellulose with enhanced ion transport properties. *J Appl Polym Sci* 139:1–17. <https://doi.org/10.1002/app.51826>
- [40] Salleh NS, Aziz SB, Aspanut Z, Kadir MFZ (2016) Electrical impedance and conduction mechanism analysis of biopolymer electrolytes based on methyl cellulose doped with ammonium iodide. *Ionics (Kiel)* 22:2157–2167. <https://doi.org/10.1007/s11581-016-1731-0>
- [41] Bhajantri RF, Ravindrachary V, Harisha A, Crasta V, Nayak SP, Poojary B (2006) Microstructural studies on BaCl₂ doped poly(vinyl alcohol). *Polymer (Guildf)* 47:3591–3598. <https://doi.org/10.1016/j.polymer.2006.03.054>
- [42] Rani M et al (2021) Magnesium ion-conducting biopolymer electrolytes based on carboxymethyl cellulose derived from palm oil empty fruit bunch fibre. *Int J Electrochem Sci* 16:210354. <https://doi.org/10.20964/2021.03.08>
- [43] Pang SF, Wu CQ, Zhang QN, Zhang YH (2015) The structural evolution of magnesium acetate complex in aerosols by FTIR-ATR spectra. *J Mol Struct* 1087:46–50. <https://doi.org/10.1016/j.molstruc.2015.01.034>
- [44] Wang LY, Zhang YH, Zhao LJ (2005) Raman spectroscopic studies on single supersaturated droplets of sodium and magnesium acetate. *J Phys Chem A* 109:609–614. <https://doi.org/10.1021/jp0458811>
- [45] Nik Aziz NA, Idris NK, Isa MIN (2010) Solid polymer electrolytes based on methylcellulose: FT-IR and ionic conductivity studies. *Int J Polym Anal Charact* 15:319–327. <https://doi.org/10.1080/1023666X.2010.493291>
- [46] Nadour M, Boukraa F, Ouradi A, Benaboura A (2017) Effects of methylcellulose on the properties and morphology of polysulfone membranes prepared by phase inversion. *Mater Res* 20:339–348. <https://doi.org/10.1590/1980-5373-MR-2016-0544>
- [47] Maity D et al (2012) Synthesis of methylcellulose-silver nanocomposite and investigation of mechanical and antimicrobial properties. *Carbohydr Polym* 90:1818–1825. <https://doi.org/10.1016/j.carbpol.2012.07.082>
- [48] Kumar A, Negi YS, Bhardwaj NK, Choudhary V (2012) Synthesis and characterization of methylcellulose/PVA based porous composite. *Carbohydr Polym* 88:1364–1372. <https://doi.org/10.1016/j.carbpol.2012.02.019>
- [49] Gordy W (2004) A relation between bond force constants, bond orders, bond lengths, and the electronegativities of the

- bonded atoms. *J Chem Phys* 14:305–320. <https://doi.org/10.1063/1.1724138>
- [50] Liu PT, Wei XM, Liu Z (2013) Miscibility study of chitosan and methylcellulose blends in advanced. *Mater Res* 75:802–805. <https://doi.org/10.4028/www.scientific.net/AMR.750-752.802>
- [51] Wojdyr M (2010) Fityk: a general-purpose peak fitting program. *J Appl Crystallogr* 43:1126–1128. <https://doi.org/10.1107/S0021889810030499>
- [52] Aziz SB et al (2020) Compatible solid polymer electrolyte based on methyl cellulose for energy storage application: Structural, electrical, and electrochemical properties. *Polymers (Basel)* 12:1–19. <https://doi.org/10.3390/polym12102257>
- [53] Liew CW, Ramesh S (2015) Electrical, structural, thermal and electrochemical properties of corn starch-based biopolymer electrolytes. *Carbohydr Polym* 124:222–228. <https://doi.org/10.1016/j.carbpol.2015.02.024>
- [54] Mazuki NF, Fuzlin AF, Saadiah MA, Samsudin AS (2019) An investigation on the abnormal trend of the conductivity properties of CMC/PVA-doped NH_4Cl -based solid biopolymer electrolyte system. *Ionics (Kiel)* 25:2657–2667. <https://doi.org/10.1007/s11581-018-2734-9>
- [55] Aziz SB, Al-Zangana S, Woo HJ, Kadir MFZ, Abdullah OG (2018) The compatibility of chitosan with divalent salts over monovalent salts for the preparation of solid polymer electrolytes. *Results Phys* 11:826–836. <https://doi.org/10.1016/j.rinp.2018.10.040>
- [56] Sravanthi K, Sundari GS, Erothu H (2021) Development of bio-degradable based polymer electrolytes for EDLC application. *Optik (Stuttg)* 241:166229. <https://doi.org/10.1016/j.ijleo.2020.166229>
- [57] Nithya S, Selvasekarapandian S, Premalatha M (2017) Synthesis and characterization of proton-conducting polymer electrolyte based on polyacrylonitrile (PAN). *Ionics (Kiel)* 23:2767–2774. <https://doi.org/10.1007/s11581-016-1841-8>
- [58] Noor NAM, Isa MIN (2019) Investigation on transport and thermal studies of solid polymer electrolyte based on carboxymethyl cellulose doped ammonium thiocyanate for potential application in electrochemical devices. *Int J Hydrogen Energy* 44:8298–8306. <https://doi.org/10.1016/j.ijhydene.2019.02.062>
- [59] Albu AM, Maior I, Nicolae CA, Bocăneală FL (2016) Novel PVA proton conducting membranes doped with polyaniline generated by in-situ polymerization. *Electrochim Acta* 211:911–917. <https://doi.org/10.1016/j.electacta.2016.06.098>
- [60] Li M, Wang X, Wang Y, Chen B, Wu Y, Holze R (2015) A gel polymer electrolyte based on composite of nonwoven fabric and methyl cellulose with good performance for lithium ion batteries. *RSC Adv* 5:52382–52387. <https://doi.org/10.1039/c5ra07182h>
- [61] Aziz SB, Marif RB, Brza MA, Hamsan MH, Kadir MFZ (2019) Employing of trukhan model to estimate ion transport parameters in pva based solid polymer electrolyte. *Polymers* 11:1694. <https://doi.org/10.3390/POLYM11101694>
- [62] Aziz SB, Karim WO, Qadir KW, Zafar Q (2018) Proton ion conducting solid polymer electrolytes based on Chitosan incorporated with various amounts of barium titanate (BaTiO_3). *Int J Electrochem Sci* 13:6112–6125. <https://doi.org/10.20964/2018.06.38>
- [63] Bouaamlat H et al (2020) Dielectric properties, AC conductivity, and electric modulus analysis of bulk ethylcarbazole-terphenyl. *Adv Mater Sci Eng* 2020:1–8. <https://doi.org/10.1155/2020/8689150>
- [64] Al-Gunaid MQA, Saeed AMN, Siddaramaiah (2018) Effects of the electrolyte content on the electrical permittivity, thermal stability, and optical dispersion of poly(vinyl alcohol)-cesium copper oxide-lithium perchlorate nanocomposite solid-polymer electrolytes. *J Appl Polym Sci* 135:45852. <https://doi.org/10.1002/app.45852>
- [65] Arya A, Sharma AL (2018) Structural, electrical properties and dielectric relaxations in Na^+ -ion-conducting solid polymer electrolyte. *J Phys Condens Matter* 30:165402. <https://doi.org/10.1088/1361-648X/aab466>
- [66] Nofal MM, Aziz SB, Ghareeb HO, Hadi JM, Dannoun EMA, Al-Saeedi SI (2022) Impedance and dielectric properties of PVC: NH_4I solid polymer electrolytes (SPEs): steps toward the fabrication of SPEs with high resistivity. *Materials* 15:2143. <https://doi.org/10.3390/ma15062143>
- [67] Ramani R, Ramachandran R, Amarendra G, Alam S (2015) Direct correlation between free volume and dielectric constant in a fluorine-containing polyimide blend. *J Phys Conf Ser*. <https://doi.org/10.1088/1742-6596/618/1/012025>
- [68] Aziz SB, Abdullah OG, Saeed SR, Ahmed HM (2018) Electrical and dielectric properties of copper ion conducting solid polymer electrolytes based on chitosan: CBH model for ion transport mechanism. *Int J Electrochem Sci* 13:3812–3826. <https://doi.org/10.20964/2018.04.10>
- [69] Tsonos C (2019) Comments on frequency dependent AC conductivity in polymeric materials at low frequency regime. *Curr Appl Phys* 19:491–497. <https://doi.org/10.1016/j.cap.2019.02.001>
- [70] Pal P, Ghosh A (2018) Investigation of ionic conductivity and relaxation in plasticized PMMA- LiClO_4 solid polymer

- electrolytes. *Solid State Ionics* 319:117–124. <https://doi.org/10.1016/j.ssi.2018.02.009>
- [71] Pritam AA, Sharma AL (2019) Dielectric relaxations and transport properties parameter analysis of novel blended solid polymer electrolyte for sodium-ion rechargeable batteries. *J Mater Sci* 54(9):7131–7155. <https://doi.org/10.1007/s10853-019-03381-3>
- [72] Arof AK, Amirudin S, Yusof SZ, Noor IM (2014) A method based on impedance spectroscopy to determine transport properties of polymer electrolytes. *Phys Chem Chem Phys* 16:1856–1867. <https://doi.org/10.1039/c3cp53830c>
- [73] Zainuddin NK, Rasali NMJ, Mazuki NF, Saadiah MA, Samsudin AS (2020) Investigation on favourable ionic conduction based on CMC-K carrageenan proton conducting hybrid solid bio-polymer electrolytes for applications in EDLC. *Int J Hydrog Energy* 45:8727–8741. <https://doi.org/10.1016/j.ijhydene.2020.01.038>
- [74] Hambali D, Osman Z, Othman L, Md Isa KB, Harudin N (2020) Magnesium (II) bis(trifluoromethanesulfonimide) doped PVdC-co-AN gel polymer electrolytes for rechargeable batteries. *J Polym Res* 27:159. <https://doi.org/10.1007/s10965-020-02083-8>
- [75] Wang N, Cai C, He X, Pang SF, Zhang YH (2018) Vacuum FTIR study on the hygroscopicity of magnesium acetate aerosols. *Spectrochim Acta A Mol Biomol Spectrosc* 192:420–426. <https://doi.org/10.1016/j.saa.2017.11.058>
- [76] Lin CL, Kao HM, Wu RR, Kuo PL (2002) Multinuclear solid-state NMR, DSC, and conductivity studies of solid polymer electrolytes based on polyurethane/poly(dimethylsiloxane) segmented copolymers. *Macromolecules* 35:3083–3096. <https://doi.org/10.1021/ma012012q>
- [77] Aziz SB, Abdullah OG, Rasheed MA (2017) Structural and electrical characteristics of PVA:NaTf based solid polymer electrolytes: role of lattice energy of salts on electrical DC conductivity. *J Mater Sci: Mater Electron* 28:12873–12884. <https://doi.org/10.1007/s10854-017-7117-x>
- [78] Ponraj T, Ramalingam A, Selvasekarapandian S, Srikumar SR, Manjuladevi R (2021) Plasticized solid polymer electrolyte based on triblock copolymer poly(vinylidene chloride-co-acrylonitrile-co-methyl methacrylate) for magnesium ion batteries. *Polymer Bulletin* 78:35–57. <https://doi.org/10.1007/S00289-019-03091-5/FIGURES/13>
- [79] Basha SKS, Rao MC (2018) Spectroscopic and electrochemical properties of PVP based polymer electrolyte films. *Polym Bull* 75:3641–3666. <https://doi.org/10.1007/s00289-017-2229-2>

Publisher's Note Springer Nature remains neutral with regard to jurisdictional claims in published maps and institutional affiliations.